The Impact of the Integrated Sachs-Wolfe Effect on Gravitational Waves

Hugo Johansson
hugo.johansson@outlook.com

under the direction of
Adam Johansson Andrews
Department of Physics
Stockholm University

Research Academy for Young Scientists
July 14, 2021

Abstract

Gravitational waves arise when a mass is accelerated and causes ripples in spacetime. When gravitational waves travel between two points, they are affected by the evolving matter they pass through. The differences in the received wave compared to the emitted wave due to these gravitational effect are described by the Sachs-Wolfe and integrated Sachs-Wolfe effects. This paper describes a method of computing these effects for a realisation of the cosmic dark matter field. The method is applied to mock merger events and dark matter fields to determine its reliability. Then, it is applied to data from the GW200105 merger event and a reconstruction of the dark matter field based on galaxy survey data from SDSS3/BOSS. The results show the increase in estimated chirp mass due to these effects to be $0.001\,29\%$ or $4.684\,503\,8 \times 10^{-5} \mathrm{M}_{\odot}$ for GW200105.

Acknowledgements

First, I wish to acknowledge Adam Johansson Andrews' contributions ranging from his deep knowledge of the subject to his very useful feedback and more. Without his assistance, this study would not have been possible. I would also like to thank Rays and their collaborative partners Kjell & Märta Beijers Stiftelse and AstraZeneca for making these four weeks possible. Finally, I wish to express my gratitude towards the organizers of Rays, not least for their feedback during the writing of this paper.

Contents

1 Introduction

In 1916, Albert Einstein developed the General Theory of Relativity, which predicts the existence of Gravitational Waves (GWs) [1]. GWs allow the study of black holes and other parts of the Universe in a way electromagnetic waves do not [2]. GWs propagate at the speed of light and contain information about their origins, but also about the large-scale structures (LSS) they have interacted with [1, 3]. Since the large-scale structure of the Universe affects the frequency, amplitude, and phase of GWs, there will also be non-negligible impacts on the calculations of luminosity, frequency, and chirp mass of the binary supermassive black holes emitting the GWs [3]. This paper will provide a first estimate of the size of these effects.

1.1 Einstein's Field Equations

Einstein's field equations describe the relationship between spacetime and the distribution of mass [4]. Spacetime is the quantity for the physical distance between points, a combination of the three dimensions of space and time [4, 5]. When a photon moves through spacetime, it follows a geodesic, the shortest path between two points in four-dimensional spacetime [5]. In Equation (1), the left side of the equality signifies the warping of spacetime, while the right side is the mass distribution. Because mass and energy are interchangeable, as $E = mc^2$, T can also represent the energy distribution. [4] This is also true for objects with a mass, which always warp spacetime [6].

$$R_{\mu\nu} - \frac{1}{2} g_{\mu\nu} R = \frac{8\pi G}{c^4} T_{\mu\nu} \tag{1}$$

where $T_{\mu\nu}$ is the stress-energy tensor, G is the gravitational constant, $g_{\mu\nu}$ is the metric tensor, $R_{\mu\nu}$ is the Ricci tensor and R is the Ricci scalar. [4]

1.2 The Einsteinian and Newtonian Viewpoints

Gravity is the dominant force at cosmological scales, from about 100 Mpc. The electrostatic force is the only other force working at these distances, but as the Universe is electrically neutral at these scales, the electrostatic force does not affect the evolution of the Universe. In this Newtonian view, gravity is caused by massive objects pulling on each other. However, the Einsteinian viewpoint assumes that gravity is simply an effect of the curvature of spacetime. While Einstein and Newton imagined what was occurring very differently, their equations give very similar results in all but what Einstein would call the strongest curvatures in spacetime. In those situations, the Einsteinian general relativistic model gives better results. When there are no deep warps in spacetime, Newtonian physics, including Poisson's equation (2), provide accurate solutions. [5]

$$\nabla^2\Phi = 4\pi G\rho \tag{2}$$

where Φ is the gravitational potential, ρ is the mass density, and G is the gravitational constant. [5]

1.3 The Friedmann–Lemaître–Robertson–Walker Metric

The structure of the Universe can be described as planets orbiting stars located in galaxies. Galaxies in turn are part of clusters, which exist inside superclusters. Yet, the Universe is *homogeneous* and *isotropic* at scales larger than 100 Mpc. [7] Isotropic means that whichever direction an observer would look, they would see roughly the same thing. Homogeneity implies that the observer can be in any location, and from that point it would still be isotropic [5]. This is assumed in the Friedmann–Lemaître–Robertson–Walker (FLRW) metric. The discovery of the cosmic microwave background (CMB) was major evidence for this theory [7]. Equation (3) shows the FLRW metric in spherical coordinates [4].

$$ds^2 = -c^2dt^2 + a^2(t)\left[\frac{dr^2}{1-kr^2} + r^2(d\theta^2 + \sin^2\theta d\phi^2)\right] \tag{3}$$

where ds is the difference in comoving distance, c is the speed of light, dt is the difference in time, $a(t)$ is the scale factor, k is the curvature constant and r, θ and ϕ are spherical coordinates. [4]

1.4 The Friedmann Equations

The Friedmann equations were derived from Einstein's field equations, using the FLRW metric [8, 7]. They describe the expansion and/or contraction of the Universe [4]. This is done using the scale factor, $a(t)$, as a function of time, by relating $a(t)$, k, R_0 and $\varepsilon(t)$ [4, 5]. The curvature constant, k, describes if the curvature is positive, negative, or flat. A flat space is one in which Euclidean geometry applies, for example meaning that a straight line is always the shortest path between two points and that the universe is infinite in size. In this case, $k = 0$. If the value of k is positive, space is spherical and no longer described by Euclidean geometry. It is also finite in size. A hyperbolic, or negatively curved, space also breaks Euclidean geometry, however, it is infinite in size, like flat space [4]. The curvature radius is expressed as R_0 and the energy density as $\varepsilon(t)$ [5]. The scale factor thus depends on the contents of the Universe. In accordance with both observations and the first (4) and second (5) Friedmann equations, galaxies move further apart at scales of tens of Mpc. Equation (4) describes how $a(t)$ changes with time, while Equation (5) describes the acceleration of $a(t)$. If the cosmological constant, Λ, is positive, it will act as a repulsive force and if the repulsive force is large enough, it will overcome gravity and therefore cause an accelerating universe. [4]

$$\left(\frac{\dot{a}}{a}\right)^2 = \frac{8\pi G}{3}\rho - \frac{kc^2}{a^2} \tag{4}$$

$$\frac{\ddot{a}}{a} = -\frac{4\pi G}{3}\left(\rho + \frac{3p}{c^2}\right) + \frac{\Lambda}{3} \tag{5}$$

where G is the gravitational constant, c is the speed of light, ρ is the mass density, Λ is the cosmological constant, k is the curvature constant, p is the pressure and $\dot{a}$ and $\ddot{a}$ are the first and second derivatives, respectively.

1.5 ΛCDM

The Λ Cold Dark Matter (ΛCDM) model is the current standard model of cosmology. It explains observations, such as the cosmic microwave background and the large-scale structure of the Universe, using the general theory of relativity [9]. ΛCDM assumes that the universe is homogeneous and isotropic [8]. To explain the accelerating expansion of the universe, it includes a kind of energy called dark energy. It also contains a material called cold dark matter, which only interacts through gravitation [10]. There also exists radiation, relativistic particles and baryonic matter. Baryonic matter is thought to only make up about 5 % of the total density, which would be approximately one fifth as much as there is non-baryonic matter. It is the cosmological constant that makes up the majority of the total density. The model also stipulates that the Universe is flat. While it is impossible to prove that it is perfectly flat, no curvature has been detected. Using the standard model, the Universe has been dated to about 14 billion years and is expected to continue ageing and expanding forever, instead of recollapsing or being static. Using all of these principles ΛCDM describes a possible past, current, and future evolution of the Universe [8].

1.6 The Sachs-Wolfe effect

The Sachs-Wolfe (SW) effect describes the effect large-scale structures have on the energy, or temperature, of photons. If the EM radiation is instead expressed as a wave, the SW effect would change its frequency [3]. The integrated Sachs-Wolfe (iSW) effect is due to the changes to gravitational anisotropies, more specifically, differences in gravitational potential Φ, over time. The equation for the iSW effect is shown in Equation (6) [11].

$$I_{isw} = \int_e^r \partial_\tau \Phi d\lambda \tag{6}$$

where ∂_τ is the partial derivative according to proper time and λ is the affine parameter describing the path between e and r. [11]

When a photon enters a gravitational well, which has a lower gravitational potential, its energy increases. This is shown as ΔE_{Entry} in Figure 1. If the universe doesn't expand while the photon is traversing it, the photon will lose exactly as much energy when exiting the gravitational well, shown as $\Delta E_{Entry} = \Delta E_{Exit} + \Delta E$. In this first scenario, the photon follows the black path. When the Universe is dominated by dark energy, the differences in gravitational potential can change with time, leading to its flattening. The gravitational potential after flattening is shown with a red line in Figure 1. When the gravitational well flattens as a wave is traversing it, it may follow a path more similar to the blue wave, thus gaining the energy $\Delta E = \Delta E_{Entry} - \Delta E_{Exit}$. Similarily, a photon would instead lose energy if it was traversing a flattening gravitational potential hill [11].

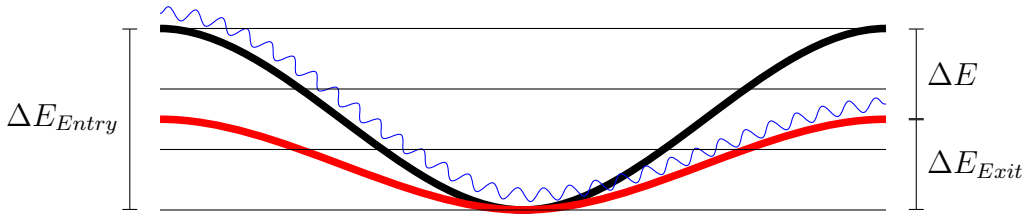

Figure 1: A GW traversing a spacetime overdensity/well. The black line represents the path of a GW before expansion and the red line is the path of a GW after expansion. The blue wave depicts a GW traversing a flattening gravitational well and thus gaining energy.

The Sachs-Wolfe effect can also be adapted for GWs, as they experience the Sachs-Wolfe and integrated Sachs-Wolfe (iSW) effects too. The phase and frequency of GWs are affected by the iSW effect similarly to CMB photons, allowing a similar use of the effect for GWs. While the corresponding iSW effect will not impact the ability to detect GWs, it does affect the resulting estimate for chirp mass, orbital frequency and luminosity distance [3]. *Luminosity distance* is the distance an object appears to be at, based on the intensity of the light. However, multiple factors, except for the inverse square law, cause the received intensity, and therefore perceived distance to the source, to be offset. Among these are the expansion of the Universe and redshift. The perceived distance will therefore be larger than it actually is. Type 1a supernovae are used as guidelines for distance, as the light they emit is always very similar [4]. The chirp mass is a specific combination of

the two masses in a binary system [12].

1.7 Black Holes

Black holes form when stars with a mass of at least 3 solar masses collapse at the end of their lives. Nothing, including light, can escape from black holes, as the escape velocity needed is larger than the speed of light. Anything which enters the event horizon will be pulled towards the centre, where a singularity is located, which warps spacetime to infinity [7]. Black holes can also merge, which is when a binary system of two black holes becomes one, more massive, black hole [13]. Some black holes classify as supermassive, such as the one at the centre of our galaxy, with a mass of about 4.3 million solar masses [7].

Binary systems of black holes provide a predictable source of GWs for waveform modelling [9]. The large masses and accelerations involved in the merger of supermassive black holes have allowed GWs to be detected [6]. When the orbits of these binary systems decay, GWs are emitted, releasing some of their orbital energy [2]. The GWs may be measurable multiple Gpc from the origin, when two large black holes with different masses coalesce. These mergers, together with more sensitive equipment, will allow for studying larger redshifts, corresponding to events further away and back in time. When a mass is accelerated, it creates GWs, which grow with increasing mass and acceleration. When the mass and acceleration are large enough, they will be measurable by current technology. Thus, binary black holes, or neutron stars, during a merger represent the best candidates for measuring GWs. The merger consists of three phases: inspiral, merger, and ringdown. The inspiral phase is when the bodies in the binary system spiral in closer. This then results in them merging into one body. The final stage of the merger is the ringdown, when gravitational waves are emitted at a higher frequency as the black hole becomes more stable [6].

A Doppler shift is the consequence of objects moving apart or towards each other. A redshift is a Doppler shift caused by objects moving apart and can be used as a unit of

time and expansion. A redshift of $z = 1$ indicates that the Universe has doubled in size since that point in time [14]. The light of an object moving away from an observer causes its spectrum to be shifted. $z = \frac{\lambda_r}{\lambda_e} - 1$ expresses the redshift as a function of the received wavelength λ_r and the emitted wavelength λ_e [7].

1.8 Observations of Gravitational Waves

While potential black hole candidates have repeatedly been found using electromagnetic observations, it was not until 2015, nearly 100 years after Albert Einstein's first prediction, that a merger of two black holes was observed. The GWs from the event referred to as GW150914 were consistent with expectations for an inspiral, merger and then ringdown of two black holes. During the 0.2s of the event, the frequency increased from 35Hz to 150 Hz during 8 cycles, with a simultaneous increase in amplitude. [1]

To measure the small changes to spacetime caused by GWs, special detectors consisting of two perpendicular, 4 km long, tunnels with mirrors are used. By projecting a laser, which is then split into two beams, one for each tunnel, any large enough change to spacetime will affect the length of the tunnels and thereby also the phase difference of the laser beams. To reduce the risk of interference, two separate detectors were built in different locations to verify the results. Having multiple detectors also allows for approximating the direction of origin for GWs. Multiple environmental sensors, such as magnetometers and radio receivers, are also used to monitor the surrounding area for events that might invalidate the results. [1]

This allowed the Laser Interferometer Gravitational-Wave Observatory (LIGO) detectors to receive GW150914 in 2015 [1]. It was the difference between a precision of $2 \times 10^{-23}/\sqrt{\text{Hz}}$ and $8 \times 10^{-24}/\sqrt{\text{Hz}}$ that allowed the GWs to be detected [15]. Future prospects for the measurement of gravitational waves include the Laser Interferometer Space Antenna (LISA) which consists of 3 spacecraft forming a triangle with sides of 5 million km [16]. Another mission, called Euclid, aims to measure dark matter and dark energy, while the Large Synoptic Survey Telescope (LSST) aims to map tens of billions

of stars and galaxies [17, 18].

1.9 BORG Data

The reconstruction of the density field used in this paper is based on the Sloan Digital Sky Survey III/Baryon Oscillation Spectroscopic Survey Data Release 12 [19]. Using galaxy redshift data and models of gravitational structure formation, the Bayesian Origin Reconstruction from Galaxies (BORG) algorithm models density fields. Gravitational structure formation is when the gravitational effects attract matter, causing the mass, and therefore gravitational force, to increase and in turn attract even more matter. Forward modelling allows the algorithm to infer non-linear features and higher-order statistics in density fields. For more information about the BORG algorithm, readers are referred to the literature [20].

1.10 The Aim of the Study

This study examines the impacts of the Sachs-Wolfe effect and the integrated Sachs-Wolfe effect on GWs, including from the neutron star-black hole binary GW observation GW200105. It is based on Equations (6) and (7) described by Laguna et al. [3]. Simulating the SW and iSW effects on GWs using BORG density field data is a novel application. This study aims to find the difference in apparent chirp mass of a binary black hole merger, known as $\chi = \frac{\delta\mathcal{M}}{\mathcal{M}_z} = -\frac{\delta f}{f_z}$, where a z index indicates redshifted values.

$$\chi = \Phi|_e^r - \vec{n} \cdot \vec{v}|_e^r - I_{isw} \tag{7}$$

where χ is the change to chirp mass ($\frac{\delta\mathcal{M}}{\mathcal{M}_z}$) or frequency ($-\frac{\delta f}{f_z}$), $\Phi|_e^r$ is the difference in gravitational potential, I_{isw} is the iSW effect and $\vec{n} \cdot \vec{v}|_e^r$ is the Doppler correction.

2 Method

The method presented below is used for three baseline tests and for one computation of observational data, with only minor differences. These differences are described in the corresponding subsections.

2.1 Outline of Algorithm

The method was based on a simulation, which generated a data cube of voxels containing a density field. Next, the gravitational potential, Φ, of the data cube was computed from the density field, with the help of a Fourier transform. The iSW effect was computed in all voxels. Then, the locations of an observer r and a source of gravitational waves e were specified. A line was drawn between e and r, along which a Riemann sum was computed using tri-linear interpolation for a better approximation. A Riemann sum was used instead of an integral because the data model was discrete.

Next, the Sachs-Wolfe effect was also calculated, using the difference in gravitational potential between r and e. The difference in relative velocity, and thus the Doppler shift correction, between e and r was assumed to be 0.

Using this information, $\chi = \frac{\delta \mathcal{M}}{\mathcal{M}_z} = -\frac{\delta f}{f_z}$ was calculated, which was the effect of the LSS on the GWs. The structure of the script is shown in Figure 2. Table 1 shows the parameters used in the different tests and illustrations of the directions of the black hole merger can be found in Appendix A.

Table 1: Method specifications. The rows represent the separate tests.

	Ascension	Declination	d_L	M_z	Cube/grid size
Zero density	30°	−70°	1500	43	4000/128
Underdensity	30°	−70°	1500	43	4000/128
Gaussian	30°	−70°	1500	43	4000/128
BORG data	106.8018°	41.8359°	265.0966	$3.619^{+0.006}_{-0.006}$ [21]	4000/256

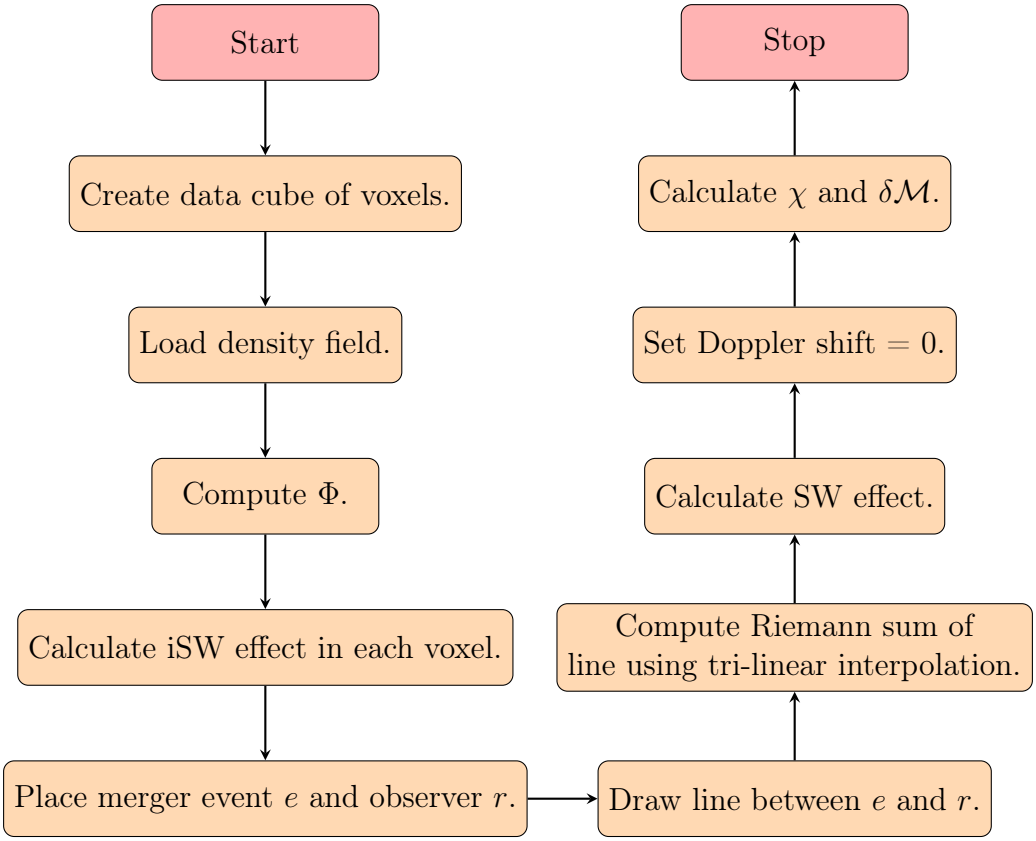

Figure 2: A flowchart for the algorithm used to compute the SW and iSW effects.

Slices of the density fields used are shown in Figure 3.

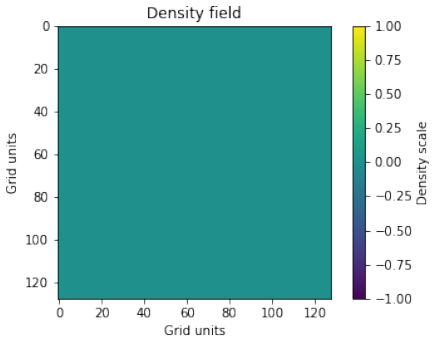

(a) A graph showing an empty toy mass density field.

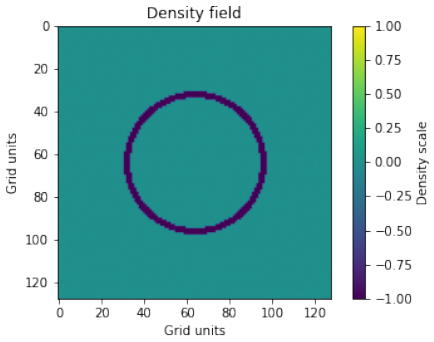

(b) A graph showing a toy mass density field with a spherical underdensity.

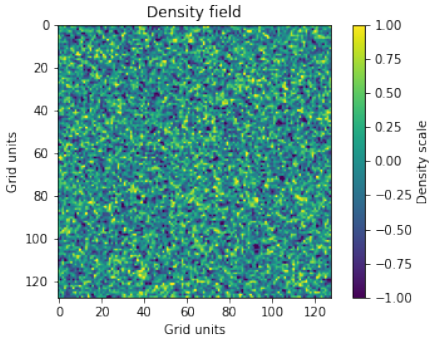

(c) A graph showing a gaussian distributed toy mass density field.

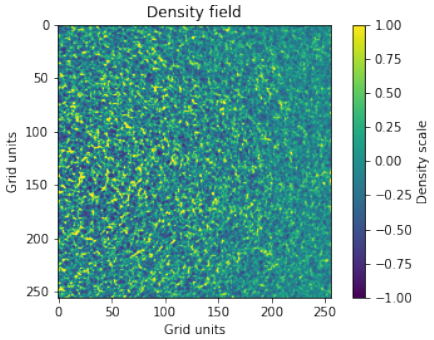

(d) A graph showing a BORG mass density field.

Figure 3: Density fields for the different scenarios.

Figure 4 shows the data used for approximating the direction of the GW200105 merger event.

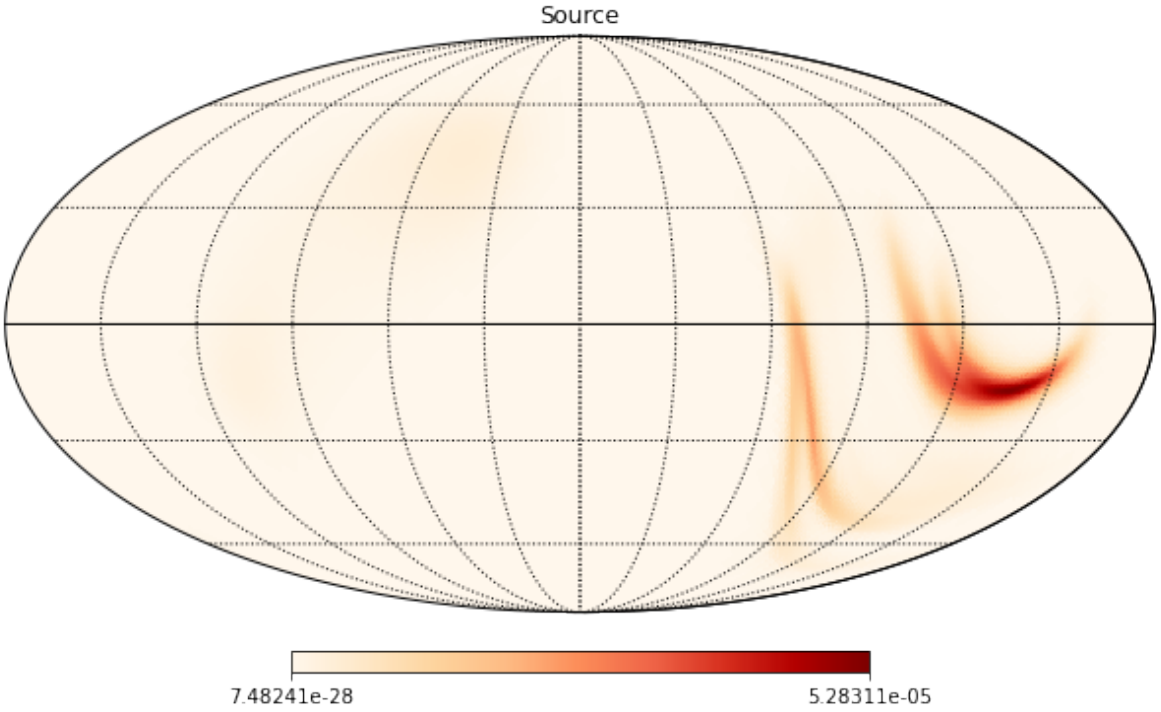

Figure 4: A map showing the probability for different merger event directions.

2.2 Baseline Test

A baseline test was performed to verify the results against expected values using known density fields. The aim of the baseline test was to determine the reliability of the method. Multiple mock density fields were tried, including:

1. An empty density field.
2. A density field with a spherical underdensity at about 1000 Mpc from the centre.
3. A Gaussian distributed density field.

The merger event location e, observer location r, chirp mass M_z and luminosity distance d_L were the same during all tests.

2.3 Observational Data

The observational data is from a data set provided by [22], which was inferred using the BORG algorithm described in subsection 1.9. Information about the direction of the selected merger event was retrieved from Beyestar data published by LIGO [23], while the chirp mass, shown in table 1, was manually retrieved from a separate source describing GW200105.

Figure 4 shows the probability for the different locations the gravitational wave may have come from. The visualised data was processed as a part of the observational data.

3 Results

Table 2 shows the resulting values from the baseline tests and the BORG simulation.

Table 2: Simulation results from density fields.

	Empty	Underdensity	Gaussian	BORG data
SW	0	$-9.692\,133\,3 \times 10^{-4}$	$-1.133\,899\,9 \times 10^{-5}$	$1.348\,252\,2 \times 10^{-5}$
iSW	0	$1.629\,088\,4 \times 10^{-4}$	$4.409\,767\,2 \times 10^{-6}$	$5.383\,279\,3 \times 10^{-7}$
χ	0	$-1.132\,122\,2 \times 10^{-3}$	$-1.574\,876\,7 \times 10^{-5}$	$1.294\,419\,4 \times 10^{-5}$
$\delta\mathcal{M}$ ($M_\odot$)	0	$-4.868\,125\,3 \times 10^{-2}$	$-6.771\,969\,6 \times 10^{-4}$	$4.684\,503\,8 \times 10^{-5}$

The density fields shown in Figure 3 are slices of the density fields. Figure 3a shows that the empty density field is zero at all points, while Figure 3b shows a spherical underdensity at about half the distance to the edge of the dataset. The Gaussian distributed density field is visualised in Figure 3c and the density field used in the observational data is shown in Figure 3d.

Figure 5 shows the integrated Sachs-Wolfe effect in all directions from the observer to the same distance as the source. Figure 5a illustrates that there is no effect in any direction, while the other three figures show varying iSW effects (non-zero values).

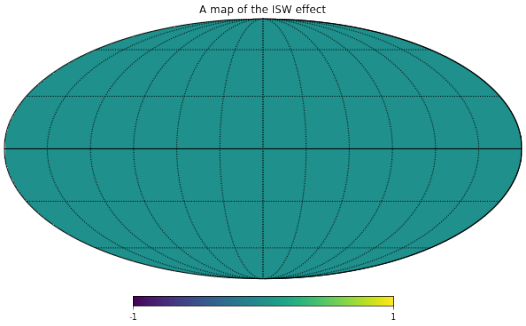

(a) Zero density field

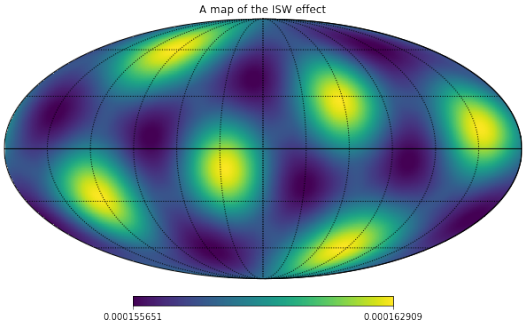

(b) Underdensity field

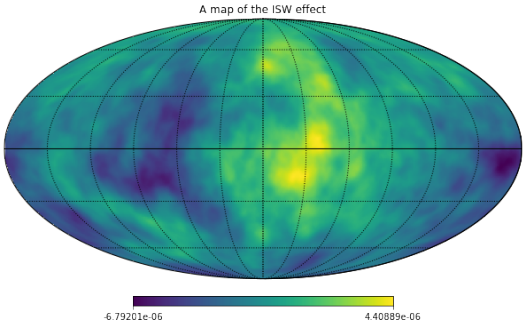

(c) Gaussian distributed density field

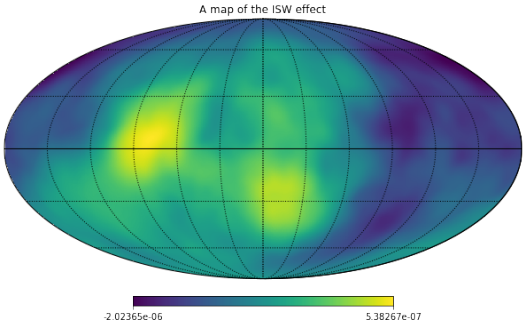

(d) BORG density field

Figure 5: Maps showing the integrated Sachs-Wolfe effect for different density fields in all directions to the distance of the black hole merger in all directions.

4 Discussion

The baseline tests gave plausible results, thus contributing to the reliability of the results from the observational data. The arguments for this conclusion are outlined in subsection 4.1.

4.1 Baseline Test

The results from the empty density field, visualised in Figure 3a, showed no SW nor iSW effect. This follows expectations, as no gravitational perturbations were modelled, as can be seen in Figure 5a. Thus, $\delta\mathcal{M}$ was also zero. As the SW and iSW effects are caused by changes to spacetime perturbations, which are in turn caused by changes in mass, these results are in favor of the model.

The spherical underdensity field showed a negative SW effect, but a positive iSW effect. This caused a negative χ, which contributed a decrease of about 0.113% to the received chirp mass and an increase to the wavelength by the same percentage. These results also follow expectations, as an underdensity causes a gravitational hill, which in turn causes the gravitational wave to lose energy in a model adhering to ΛCDM. The decrease in mass was approximately $0.0487\,\mathrm{M}_\odot$. The results from the Gaussian distributed field showed a negative SW effect and a positive iSW effect, resulting in a negative χ. The decrease in received chirp mass would thus be about 0.00157%, or $6.77 \times 10^{-4}\,\mathrm{M}_\odot$.

In a perfectly spherical underdensity field the SW and iSW effects would be expected to be constant to all points outside the sphere. However, Figure 5b shows a difference in the iSW effect depending on the direction. This is likely caused by the underdensity field not being a perfect sphere. Instead, it is made up of cubic voxels. Depending on if the line between e and r passes through a voxel perpendicularly or at a 45° angle, the length of the intersection with the underdensity will vary. A higher-resolution density field would be expected to reduce its effect, however, a spherical coordinate system would have to be implemented to fully eliminate this effect, as opposed to the Cartesian coordinate system

used in the simulation.

4.2 Observational Data

As the method passed the baseline test, an analysis of the observational data can be carried out. For the observational data, the results showed a positive SW effect and a positive iSW effect. This resulted in a positive value for χ, which would cause an increase in received chirp mass of about 0.00129%, or $4.68 \times 10^{-5}\,\mathrm{M}_{\odot}$, and a decrease in the frequency of the same percentage.

This study did not take into account anything except the line of sight BORG data. Other cosmological phenomenon, such as gravitational lensing, were ignored. The BORG data also does not include baryonic matter, which likely affected the properties of the GWs received by LIGO. The Doppler shift due to a difference in the peculiar velocities was assumed to be 0, which is likely inaccurate. An improved model would have to take into account this Doppler shift to provide more accurate results. This could be examined in a future study.

The value for the difference in received chirp mass of $4.68 \times 10^{-5}\,\mathrm{M}_{\odot}$ is smaller than the uncertainty in the estimated chirp mass by about 100 times. Thus, the real-world applications of these results are very limited. When new instruments in the future provide more accurate data, calculating these effects may prove valuable.

Next-generation telescopes will improve the data and understanding necessary to make these estimations. Euclid aims to explore the dark energy responsible for the accelerating expansion of the universe. The Rubin Observatory's Legacy Survey of Space and Time will study billions of stars and galaxies, which has the potential to improve the data the BORG algorithm uses. The Laser Interferometer Space Antenna (LISA) is a laser interferometer, like LIGO, but located in space. Instead of the 4 km long tunnels at LIGO, LISA will consist of three separate spacecraft with millions of kilometres between them. This more accurate data would likely allow for more accurate estimations of the properties of merger events, such as the chirp mass, but also the SW and iSW effects.

4.3 Conclusion

The plausibility of the results presented in this paper is very hard to establish, as this is the first study to provide an estimate of the impact of the Sachs-Wolfe and the integrated Sachs-Wolfe effects on gravitational waves for different realisations of the density field. The results showed an increase in chirp mass of 0.00129% or $4.68 \times 10^{-5}\,\mathrm{M}_{\odot}$. If these results are accurate, their small effects compared to the uncertainty in the detector-frame chirp mass make them negligible in estimations of the chirp mass.

References

[1] Abbott BP, Abbott R, Abbott T, Abernathy M, Acernese F, Ackley K, et al. Observation of gravitational waves from a binary black hole merger. Physical review letters. 2016;116(6):061102.

[2] Kokkotas K, et al. Gravitational waves. Acta Physica Polonica B. 2007.

[3] Laguna P, Larson SL, Spergel D, Yunes N. Integrated Sachs–Wolfe Effect for Gravitational Radiation. The Astrophysical Journal Letters. 2010;715(1):L12.

[4] Liddle A. An introduction to modern cosmology. John Wiley & Sons; 2015.

[5] Ryden B. Introduction to cosmology. Cambridge University Press; 2017.

[6] Flanagan EE, Hughes SA. The basics of gravitational wave theory. New Journal of Physics. 2005;7(1):204.

[7] Natario J. General relativity without calculus: a concise introduction to the geometry of relativity. Springer Science & Business Media; 2011.

[8] Liddle AR. An introduction to modern cosmology. 2nd ed. Chichester: Wiley; 2003.

[9] Cai RG, Cao Z, Guo ZK, Wang SJ, Yang T. The gravitational-wave physics. National Science Review. 2017;4(5):687–706.

[10] Giovannini M. Theoretical tools for CMB physics. International Journal of Modern Physics D. 2005;14(03n04):363–510.

[11] Giannantonio T, Scranton R, Crittenden RG, Nichol RC, Boughn SP, Myers AD, et al. Combined analysis of the integrated Sachs-Wolfe effect and cosmological implications. Physical Review D. 2008;77(12):123520.

[12] Abbott BP, Abbott R, Abbott T, Abernathy M, Acernese F, Ackley K, et al. Properties of the binary black hole merger GW150914. Physical review letters. 2016;116(24):241102.

[13] Collaboration LS, Collaboration V, et al. The basic physics of the binary black hole merger GW150914. Annalen der Physik. 2017;529(1-2):1600209.

[14] Cheng TP. Relativity, gravitation and cosmology: a basic introduction. vol. 11. Oxford University Press; 2009.

[15] Martynov DV, Hall E, Abbott B, Abbott R, Abbott T, Adams C, et al. Sensitivity of the Advanced LIGO detectors at the beginning of gravitational wave astronomy. Physical Review D. 2016;93(11):112004.

[16] Danzmann K, Rüdiger A. LISA technology—concept, status, prospects. Classical and Quantum Gravity. 2003;20(10):S1.

[17] Racca GD, Laureijs R, Stagnaro L, Salvignol JC, Alvarez JL, Criado GS, et al. The Euclid mission design. In: Space telescopes and instrumentation 2016: optical, infrared, and millimeter wave. vol. 9904. International Society for Optics and Photonics; 2016. p. 99040O.

[18] Ivezić Ž, Kahn SM, Tyson JA, Abel B, Acosta E, Allsman R, et al. LSST: from science drivers to reference design and anticipated data products. The Astrophysical Journal. 2019;873(2):111.

[19] Eisenstein DJ, Weinberg DH, Agol E, Aihara H, Prieto CA, Anderson SF, et al. SDSS-III: Massive spectroscopic surveys of the distant universe, the Milky Way, and extra-solar planetary systems. The Astronomical Journal. 2011;142(3):72.

[20] Jasche J, Wandelt BD. Bayesian physical reconstruction of initial conditions from large-scale structure surveys. Monthly Notices of the Royal Astronomical Society. 2013 Apr;432(2):894–913. Available from: http://dx.doi.org/10.1093/mnras/stt449.

[21] Abbott R, Abbott TD, Abraham S, Acernese F, Ackley K, Adams A, et al. Observation of Gravitational Waves from Two Neutron Star–Black Hole Coalescences. The Astrophysical Journal Letters. 2021 Jun;915(1):L5. Available from: http://dx.doi.org/10.3847/2041-8213/ac082e.

[22] Lavaux G, Jasche J, Leclercq F. Systematic-free inference of the cosmic matter density field from SDSS3-BOSS data. arXiv preprint arXiv:190906396. 2019.

[23] S200105ae. LIGO Scientific Collaboration;. Accessed: 2021-07-13. https://gracedb.ligo.org/superevents/S200105ae/.

A Directions of the signals

Figure 6-9 show the direction of the black hole merger e as seen by the observer at r. They are marked with red dots on the maps and are identical in figure 6-8.

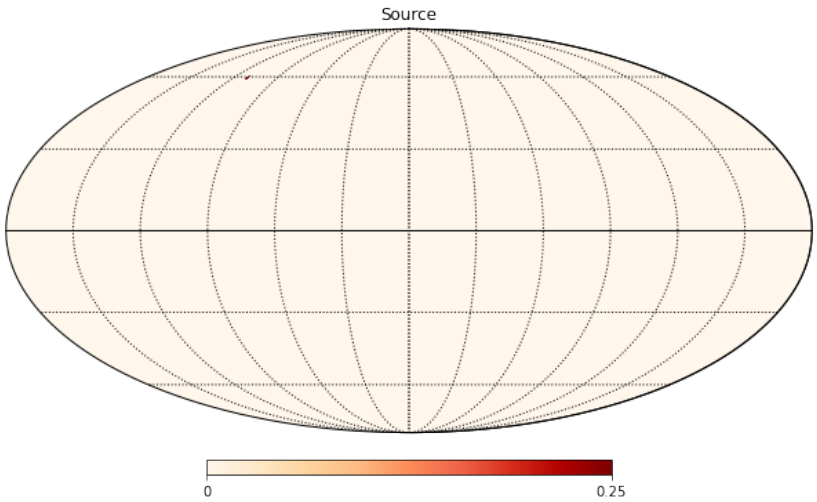

Figure 6: A map showing the direction of a toy black hole merger (shown in red).

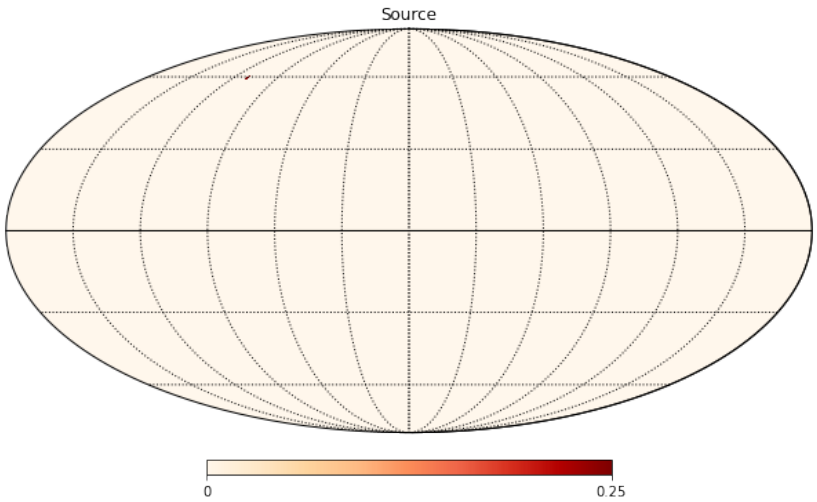

Figure 7: A map showing the direction of a toy black hole merger (shown in red).

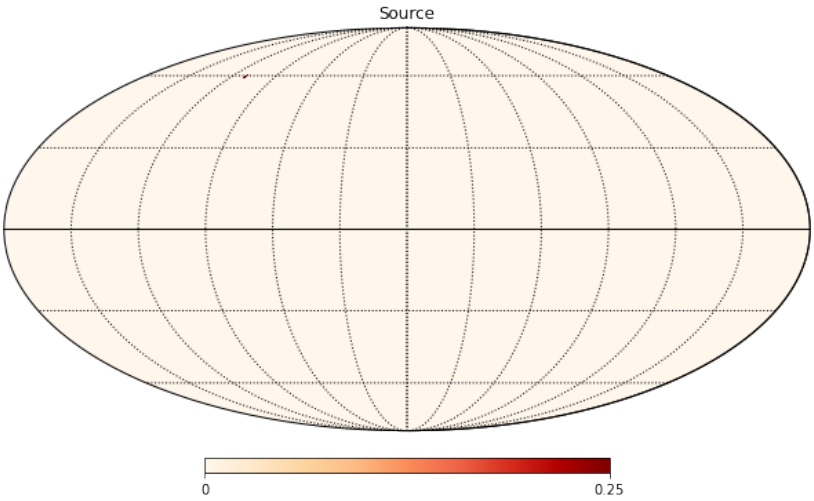

Figure 8: A map showing the direction of a toy black hole merger (shown in red).

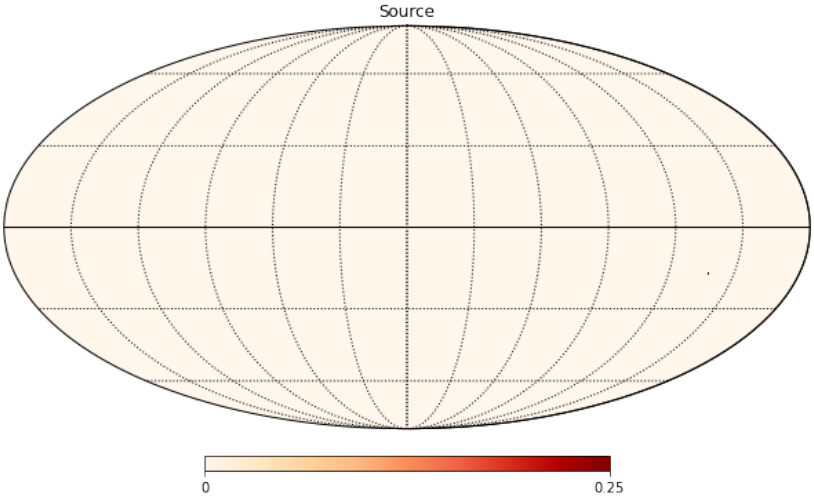

Figure 9: A map showing the direction of the GW200105 black hole merger (shown in red).